Radio Science, Volume ???, Number , Pages 1–19,

In-Situ Irregularity Identification and Scintillation Estimation using Wavelets and CINDI on C/NOFS

R. A. Stoneback,[1] R. A. Heelis,[1] R. G. Caton,[2] Y.-J. Su,[2] K. M. Groves[3]

R. G. Caton, AFRL/RVBXI, 3550 Aberdeen Ave S.E., Kirtland AFB, NM 87117, USA.

K. M. Groves, Institute for Scientific Research, Boston College, 400 St. Clements Hall, 140 Commonwealth Ave., Chestnut Hill, MA 02467, USA.

R. A. Heelis, W. B. Hanson Center for Space Sciences, 800 W. Campbell Rd. WT 15, Richardson, TX 75080, USA.

R. A. Stoneback, W. B. Hanson Center for Space Sciences, 800 W. Campbell Rd. WT 15, Richardson, TX 75080, USA. (rstoneba@utdallas.edu)

Y.-J. Su, AFRL/RVBXP, 3550 Aberdeen Ave S.E., Kirtland AFB, NM 87117, USA.

[1]W. B. Hanson Center for Space Sciences,

Wavelets are a time-domain method that is able to extract both time and frequency information from a signal. The Morlet wavelet is used here to characterize the magnitude of ionospheric irregularities using measurements of the total ion density from the Coupled Ion Neutral Dynamics Investigation (CINDI) package onboard the Communications/Navigation Outage Forecasting System (C/NOFS) spacecraft. The power in ionospheric irregularities at scale sizes less than 128 km is used to generate an irregularity amplitude index. This index is used with a phase screen analysis to form an estimate of scintillation at the satellite location. The temporal information retained in a wavelet analysis also allows for an accurate power spectrum calculation even when used on short segments of data and is useful for real-time processing of irregularity detection onboard a satellite or for analyzing the long datasets produced by a satellite. A comparison of the in-situ scintillation estimate and SCINDA measurements of the S_4 index is presented.

Physics Department, University of Texas at Dallas, Richardson, Texas.

[2]Air Force Research Laboratory, Space Vehicles Directorate, Kirtland Air Force Base, New Mexico, USA.

[3]Institute for Scientific Research, Boston College, Chestnut Hill, Massachusetts, USA.

1. Introduction

The formation of equatorial irregularities in the ionosphere can cause communications outages by disrupting waveforms as a signal travels through the irregularity. Sharp changes in ion density within and around an irregularity cause communication signals to refract as they travel through the ionosphere, distorting the waveform recorded by an observer. The Communications/Navigation Outage Forecasting System (C/NOFS) satellite carries a suite of instruments to measure a number of expected drivers for irregularity formation. In-situ measurements of total ion density by the Coupled Ion and Neutral Dynamics Investigation (CINDI) are used here to identify the location and magnitude of irregularities. To provide some validation of the extraction of irregularity amplitude from total density measurements, a in-situ estimate of S_4 is generated and compared with ground station measurements. The S_4 index [*Briggs and Parkin*, 1963] measures the root mean square fluctuations in signal intensity, normalized by the average signal intensity:

$$S_4^2 = \frac{< I^2 > - < I >^2}{< I >^2}. \tag{1}$$

In this paper we focus on determining the perturbations in ion density along the satellite track using wavelets. Wavelets are a time-domain technique useful for signal analysis and many other applications. Wavelets have been used to analyze amplitude scintillation measurements by *Wernik* [1997] and *Materassi and Mitchell* [2007] as well as to study turbulence in the high latitude ionosphere [*Lagoutte*, 1992]. A review of wavelets for geophysical applications can be found in *Kumar and Foufoula-Georgiou* [1997].

The Morlet wavelet is chosen here due to its construction using the sines and cosines present in Fourier analysis. This construction gives the Morlet wavelet a limited bandwidth that can be used to isolate variations at a particular scale size. Further, the power spectrum as well as the waveforms isolated for a particular scale size may be interpreted similarly to those produced by Fourier analysis. Thus, the results from the Morlet wavelet may be compatible with analyses and intuition based upon Fourier analysis of ionospheric irregularities.

An advantage of wavelets over the Fourier method or the Maximum Entropy Method (MEM) used by *Wernik et al.* [2007] is that time information is retained, providing greater specificity on where irregularities occur. While a Fourier or MEM analysis produces a single power spectrum when applied to a segment of data, a wavelet analysis produces a power spectrum at every measurement location in the data segment. Thus, if a data segment contains an isolated irregularity, the Fourier power spectrum will characterize both the irregularity and the variations in the background ionosphere surrounding it. Using wavelets, the power spectrum of the irregularity may be obtained utilizing only measurements from within the irregularity. This is expected to provide a more accurate description of the spectral index within the irregularity.

The retained time information also offers some practical benefits in producing an accurate characterization of density variations in a long satellite data set. Using wavelets, density measurements may be analyzed using very short segments of the data set but produce the same result as if the whole data set was analyzed at once. While the use of a short data segment will introduce errors in the wavelet convolution near the edges of the segment, these locations are known and may be ignored. By using a series of overlapping segments from the satellite track, a complete analysis of the data set may be constructed using only wavelet convolutions unaffected by edge effects, producing an accurate power spectrum for all density measurements. This technique may be used for real time processing of density measurements onboard a satellite with the same accuracy as when applied as a post-process on the ground.

Once the perturbation in ion density has been determined, it is used to estimate S_4 following the in-situ scintillation performed by *Basu et al.* [1976] for the equatorial OGO-6 satellite. *Basu et al.* [1976] implements the phase screen analysis by *Rufenach* [1975, 1976] which presumes that the irregularity follows a power law with scale size. This power law is used to relate the magnitude of irregularities at sizes measurable by the satellite to scale sizes that impact radio waves of interest. *Wernik et al.* [2007] uses *Rino* [1979a] and incorporates the IRI model to account for the location of the peak in ion density relative to the satellite to identify polar scintillation using Dynamics Explorer data. The work by *Rino* [1979a] requires a turbulence parameter which may be determined using the measured spectral index as well as the power within the irregularity at one scale size. These parameters may also be determined using the presented method.

Scaling the observed densities to those observed at the F-peak is not attempted here and is reserved for future work. Without knowledge of the full density altitude profile, the presented in-situ estimated S_4 index is expected to under report scintillation and can not be verified in an absolute sense. Further, in-situ measurements reported by *Singh and Szuszczewicz* [1984] also demonstrate changes in the spectral index based upon scale size, which are not included here. Using a single power-law scaling may over-estimate scintillation at smaller length scales [*Retterer*, 2010].

The in-situ estimate is compared against measurements of S_4 performed by SCINDA, a ground station network that measures the impact of irregularities upon VHF and GPS signals at a number of stations around the globe. A comparison of the in-situ S_4 and SCINDA measurements of S_4 at 250 MHz is presented and used to establish that wavelets are effective at identifying irregularities from total ion density measurements and the wavelet determined variance associated with the irregularity may be used as input for scintillation estimation methods.

2. Morlet Wavelet

The Morlet wavelet is used to extract changes in the Coupled Ion Neutral Dynamics Investigation (CINDI) measurements of total ion density. The Morlet wavelet

$$\Psi_\circ(\eta) = \pi^{-1/4} e^{-i\omega_\circ \eta} e^{-\eta^2/2} \tag{2}$$

is the combination of a Fourier term windowed by a gaussian, localizing the wavelet in a non-dimensional "time" parameter η [*Torrence and Compo*, 1997]. The non-dimensional frequency $\omega_\circ$ is taken to be six to satisfy the admissibility condition for wavelets [*Farge*, 1992].

This wavelet shares a similar interpretation with the standard Fourier transform, but provides greater specificity on when oscillations occur in a time series. A Fourier decomposition of a time series characterizes frequencies present throughout the entire time series. A continuous wavelet convolution of a time series is computed for each point in the series. At each point, the Morlet wavelet is centered upon the sample and a convolution is performed. The size of the Morlet wavelet is varied to investigate the presence of oscillations at different sizes while retaining the same functional form. Small scale sizes involve a small number of samples around the desired time while larger scales necessarily involve a larger range of samples. The Morlet wavelet has a total length $2\sqrt{2}s$ [*Torrence and Compo*, 1997], where s is the scale size of the wavelet.

The number of samples varies by wavelet choice, and for the Morlet wavelet this may also be varied with the choice of $\omega_\circ$. Increasing $\omega_\circ$ produces more sinusoidal periods with the gaussian time window, providing greater frequency resolution while increasing the number of elements required to identify that oscillation (decreasing time resolution). The tradeoff between frequency and temporal resolution for the Morlet wavelet implies that it will not resolve pure sinusoids as sharply as the Fourier transform. Since irregularities are sharp changes in density, this results in a broad spatial spectrum thus the increased bandwidth of a Morelt wavelet at a particular scale is not a significant disadvantage for irregularity identification or scintillation estimation.

Note that the continuous wavelet transform allows any scale size to be specified. Though constructed using sinusoids, the Morlet wavelet is limited in time by a gaussian, thus Morlet wavelets of similar but different size will extract similar information from a given signal. By applying a range of scale size wavelets, a power spectrum of the signal similar to that produced by Fourier analysis is generated.

In practical terms, by retaining time information, wavelet convolutions can be applied to short time segments of a longer signal and avoid the accuracy penalty from using short time signals. Consider a moving centered window of length n viewing a long time signal, subdividing the signal into smaller segments that are analyzed with wavelets. When each segment is analyzed the convolution of samples near the segment edges will be distorted. Since the wavelet convolution is centered upon the time to be investigated, for samples near the segment edge a portion of the wavelet will extend past the edge of the data segment, preventing an accurate characterization of the signal at that scale size and time. The choice of wavelet and scale size determines the number of samples from the edge before an accurate wavelet convolution is possible. In general, m samples will have accurate convolutions over the scale size range of interest where $m < n$. The longer the data segment, the larger the maximum scale size that may be investigated. For a fixed scale size, an increase in n leads to a larger fraction of samples that may be characterized accurately.

Since the influence of the segment edge on a wavelet is well specified, portions of a given data segment that are impacted by the edge may be ignored. If the moving window of length n only moves by m samples each iteration, then the data segments characterized by wavelets will overlap. The m samples calculated without error and extracted each iteration are sufficient to characterize the whole time signal with sufficient iterations. This method is particularly useful for real-time applications such as onboard satellite processing or analyzing very long time signals. Wavelet software provided by *Torrence and Compo* [1997] is integrated into this method to produce the results here.

The properties of the Morelet wavelet can be used to determine scale-limited variances in ion density, reconstruct perturbation waveforms in density as well as investigate the scaling properties of irregularities with size. Here, we concentrate on determining the variance in ion density as a means of identifying irregularities and use that variance as an input to a scintillation model.

3. Characterizing Irregularities

An example wavelet decomposition is shown in fig. 1. The black line in the top panel is the total ion density measured by the Retarding Potential Analyzer (RPA) on C/NOFS as part of CINDI. This density is first normalized by 10^4 cm^{-3} and the mean value of the finite sample is subtracted. The Morlet wavelet decomposition of this signal is in fig. 1b. For each sample, the complex decomposition coefficients for each scale size can be computed. Wavelet decompositions for scale sizes that extend beyond the time series are influenced by the edges of the finite sample size and are discarded as indicated by the hatched area. The line that separates these regions is known as the cone of influence.

The yellow box in the center of fig. 1b outlines the central quarter of the time series. In this region, the behavior over a constant range of scale sizes can be investigated free from edge effects that arise from the use of a finite sample size. The green line in fig. 1a is the reconstructed waveform using the wavelet convolutions for scale sizes above the cone of influence. Since the largest scale sizes have been removed, this waveform may be interpreted as the perturbation in ionospheric density. Outside the central quarter of elements, the perturbation waveform is constructed using a changing range of scale sizes and is not retained. To extract a continuous perturbation waveform over a constant range of scale sizes, the buffer is advanced by a quarter of the total elements as shown in fig. 2 and the waveform in the central quarter is again extracted.

The particulars of the C/NOFS orbit can lead to measured density changes that are not due to irregularities. In fig. 3 changes in the ion density occur for scale sizes greater than 512 km. To reduce the chance of similar waveforms, which are not related to irregularities, from being used in a scintillation estimation, only scale sizes less than 128 km are considered, equivalent to approximately 17 s of observations on CINDI at an orbital velocity near 7.6 km/s. The spacing between irregularities is generally between $100-200$ km, thus choosing 128 km as a maximum gives a density perturbation of similar magnitude to the total density depletion. A full reconstruction of the density signal requires all spatial scales. Scale sizes lower than 128 km may also be used for scintillation estimates since measurements at a particular scale are translated to smaller scales that impact signals of interest. This figure also emphasizes the interpretation of the reconstruction waveform as a density perturbation. Though the measured density is changing, these changes occur at scale sizes that are larger than the retained wavelet coefficients, thus the perturbation waveform is near zero.

The perturbation waveforms illustrated in figs. 1-3 are not the best representation for generating a scintillation estimate. The change in ion density can be positive or negative and in general the signal oscillates between these values. However, regardless of whether the change in density is an increase or decrease from surrounding values, these changes impact radio signals. The perturbation waveform has been constructed using only the real part of the Morlet decomposition. The complex magnitude of these coefficients may be used to construct a perturbation amplitude.

Parseval's Theorem for the Morlet wavelet [*Torrence and Compo*, 1997] analysis allows us to determine the variance of the measured irregularities. The Morlet wavelet power for scale sizes less than 128 km is summed, weighted by scale size and normalized appropriately [*Torrence and Compo*, 1997] to produce an equivalent perturbation amplitude at each measurement location,

$$|A|^2 = \frac{\delta j \delta t}{C} \sum_{s=7.5}^{128} \frac{P_s}{s} \tag{3}$$

where $|A|^2$ is the variance of the ionospheric irregularities and P_s is the wavelet power for scale size s. The standard deviation $|A|$ provides a positive measure of the strength of the irregularities at each measurement location. The sampling rate δt is the distance between measurements for the RPA ($\delta t = 3.75$), $\delta j = .25$ relates to the interval between the scale lengths over which the wavelet analysis is performed (4 per octave) and $C = 0.776$ [*Torrence and Compo*, 1997] is a wavelet dependent constant. The oscillatory nature of the Morlet wavelet yields an amplitude that is only half the total change in ion density at a point, thus the peak-to-peak perturbation amplitude is taken to be

$$\overline{\Delta N} = 2|A|. \tag{4}$$

4. Scintillation Estimation

The spatial changes in ion density obtained using the Morlet wavelet can be used in the scintillation estimation by *Rufenach* [1975] and used by *Basu et al.* [1976]. The outer scale size observed by CINDI (128 km) is scaled down to sizes affecting a user specified communications frequency using a three dimensional power law scaling for ionospheric irregularities with spectral index $p = 4$. The S_4 index is estimated using *Rufenach* [1975],

$$S_4 = \sqrt{2}\Phi F' f(\beta) \tag{5}$$

where F' is a Fresnel filter function, $f(\beta)$ is a geometric factor for anisotropic irregularities and Φ is the phase deviation. The phase deviation is given by

$$\Phi = \Delta N \frac{r_e \lambda}{2^{1/4}} \sqrt{\frac{\pi L_e \alpha \sec \chi}{\beta K_\circ}} \tag{6}$$

where ΔN is the magnitude of the irregularity, r_e is the classical electron radius, λ is the free space wavelength of the communications signal, L_e is the thickness of the scattering layer, α is the axial ratio of field-aligned irregularities (assumed to be greater than 5) and $K_\circ$ is the outer scale wavenumber of irregularities. The zenith angle between the wavefront and the plane of the ionosphere is χ and is taken to be 0. The remaining term, β, is the axial ratio transverse to α, defined in terms of the angle between the wavefront and the magnetic field ψ, $\beta^2 = \cos^2\psi + \alpha^2 \sin^2\psi$. Given the equatorial orbit of C/NOFS it is assumed that $\psi = \pi/2$.

The Fresnel filter function is given by

$$F' = \sqrt{1 - e^{-u}} \tag{7}$$

where

$$u = \frac{\lambda z}{2\pi} K_\circ^2 \tag{8}$$

is defined in terms of the mean distance between observer and irregularities (z) as well as the outer scale wavenumber. The Fresnel wavenumber is

$$K_f = \sqrt{\frac{4\pi}{\lambda z}} \tag{9}$$

and the geometric factor is

$$f(\beta) = \frac{\sqrt{3\beta^4 + 2\beta^2 + 3}}{\beta^2\sqrt{8}}. \tag{10}$$

Though the largest impact to a radio signal occurs at the F-peak density maximum generally located below the satellite, the height of the irregularities (z) is taken as 450 km, reflecting the average altitude of CINDI when both ion drifts and densities are available during the recent solar minimum [*Stoneback et al.*, 2011]. The and the layer thickness (L_e) is assumed to be 200 km. Using the specified parameters for the phase screen analysis, the estimated S_4 is the product of a scaling constant and the magnitude of the density perturbation associated with the irregularity.

An example pass with the perturbation amplitude for scale sizes less than or equal to 128 km is in fig. 4. The ion density measured by CINDI is in black in fig. 4 along with the $\overline{\Delta N}$ obtained using eqn. 4. Near 2000 MLT, a narrow irregularity is seen in density measurements which has a corresponding narrow spike in $\overline{\Delta N}$. Later near 2030 MLT, a long train of irregularities are seen in the density measurements. $\overline{\Delta N}$ rises to 1×10^5 cm^3 at the start of the irregularities in a background ionosphere with densities near 2×10^5 cm^3. The $\overline{\Delta N}$ remains positive over the region of irregularities observed and varies as the strength of the irregularities changes. Near 2230 MLT a weaker set of irregularities are observed with a correspondingly weaker $\overline{\Delta N}$. The estimated scintillation using the wavelet derived $\overline{\Delta N}$ is shown for VHF frequencies of 140 and 250 MHz. Before the start of irregularities, this value remains close to zero. During the train of irregularities, the S_4 estimation is distinctly elevated, identifying the whole region as disturbed.

5. SCINDA Comparison

A comparison of the scintillation estimation using the wavelet extracted $\overline{\Delta N}$ to measurements by the SCINDA ground station network is shown in fig. 5. To obtain a good correspondence between the scintillation estimation and SCINDA observations, a constant multiplicative factor of 4 had to be included with the in-situ estimate. Since C/NOFS is not measuring density perturbations at the peak in ion density and scintillation depends upon the absolute change in density, scintillation estimates are expected to underestimate the value measured on the ground. Thus, this factor is expected to depend upon the altitude of the F-peak in ion density relative to the altitude of the spacecraft though the empirical scaling may also account for limitations of the scintillation model used to estimate S_4. This factor of 4 is included only for the passes in fig. 5.

On Nov. 4, 2009 a quiet night was observed by the Kwajelein SCINDA station as shown by the blue trace in the top panel. The ground station is monitoring signals at 250 MHz with a noise floor near 0.1 on the S_4 index. The in-situ scintillation estimation using C/NOFS is in black. The scintillation estimates displayed are restricted to satellite altitudes below 550 km and are within 12° apex longitude of the magnetic flux tubes monitored by the SCINDA station. The longitudinal width was chosen so that the 15 passes made by C/NOFS over the longitude sector centered upon the SCINDA measurement location form a quasi-continuous signal in local time. Though the satellite results convolve both longitude and local time changes, only the local time is reported. The altitude of C/NOFS also varies around the orbit, though this variation is repeated each pass allowing for relative comparisons of the estimated scintillation as a function of MLT in fig. 5. The in-situ estimation shows a small amount of scintillation near midnight, reaching values near 0.1 on the estimated S_4 index.

The next day similarly quiet conditions were observed at Kwajalein (not shown), though significant irregularities were observed at other SCINDA stations. In the middle panel both C/NOFS and the Christmas Island station agree that significant scintillation at 250 Mhz started at 2100 LT. The in-situ estimation only accounts for weak-scattering [*Basu et al.*, 1976] while values above 0.4 likely involve multiple scattering events. Thus values above 0.4 for the in-situ estimated S_4 index will not accurately describe the extent of scintillation. While the scintillation estimate from C/NOFS as it repeatedly moves in and out of the longitude sector does not account for every detail in the SCINDA measurements, both the SCINDA and C/NOFS observations agree that scintillation occurred between $20 - 25$ LT. On the same night at the Cape Verde station, shown in the lower panel, scintillation was observed though not as strong as observed at Christmas Island. The lower scintillation levels are also reported by C/NOFS. Thus, relative changes in the wavelet derived in-situ irregularity amplitude are consistent with changes observed on the ground.

6. Discussion and Conclusion

The wavelet transform is an effective tool for characterizing irregularities in measurements of ion density. The wavelet decomposition presented only uses wavelet coefficients when they are unaffected by edge effects, providing an accurate description of the strength of irregularities at different scale sizes for each measurement location. The technique can be used to process very long time spans of data as well as process irregularity detection onboard a satellite in real time. The total power in irregularities below and including 128 km are summed and converted into an equivalent density perturbation amplitude using Parseval's Theorem. This density perturbation amplitude is scaled down to sizes affecting communications and an estimate of the scintillation on the ground is made using the method presented by *Rufenach* [1975].

An alternate method by *Rino* [1979a] incorporates the variance of electron density irregularities to estimate scintillation using a turbulence parameter. Used by *Wernik et al.* [2007], the one dimensional spectral power index as well as the power at a given scale size inside an irregularity is used to determine the turbulence parameter. Using wavelets, the power spectrum of an irregularity may be determined using only measurements taken within the irregularity. The size of the irregularity as well as the choice in wavelet determine the maximum scale size that may be investigated and remain within the irregularity. Isolating the spectrum of the irregularity itself should provide an accurate specification of the irregularity spectral index. Both the wavelet derived variance and spectral power could be used as inputs in scintillation estimation [*Rino*, 1979a; *Wernik et al.*, 2007].

The convolution of longitude and local time inherent in CINDI observations of the ionosphere complicates comparisons with ground based stations. To limit the influence of this convolution, CINDI measurements were restricted to a 24° longitude sector centered upon SCINDA measurement locations. However, there can be significant differences in the state of the ionosphere over 24° longitude, thus even a perfect calculation of scintillation from in-situ measurements will in general only approximate what is seen on the ground at a particular location.

Despite these complications, the in-situ estimation of scintillation displays a good correspondence with observations from the SCINDA ground station network when including an empirically determined constant multiplicative factor. The altitude range of C/NOFS ensures that irregularities will be observed at altitudes away from the peak in F-region ion density. Scintillation is driven by the magnitude of the density perturbation which decreases with distance from the peak, thus the in-situ scintillation estimation will generally underestimate the true value. By incorporating an ionospheric density model similar to *Wernik et al.* [2007], the strength of irregularities $\overline{\Delta N}/N$ at the C/NOFS altitude can be translated to the corresponding $\overline{\Delta N}_{peak}$ supposing that the irregularity was at the F-region peak. No attempt to account for the altitude variation is made here. Thus the correspondence with SCINDA only establishes that relative changes in the estimation of scintillation using CINDI are consistent with ground measurements. This is sufficient, however, to investigate climatological variations of irregularities with geophysical parameters.

The empirical scaling applied to the scintillation estimate for the SCINDA comparison is not expected to remain constant. The comparison shown demonstrates the empirical constant was suitable for scintillation estimation over 24 hours and at multiple locations around the equator. Periodic updates to this scaling may be sufficient to provide a general estimate of the equatorial distribution of scintillation in near real-time.

An intrinsic limitation to the interpretation and use of these data lie in the altitude limits of the CINDI data available. In cases where ionospheric irregularities remain at or below the F-peak and do not have strong signatures that map to the altitudes being sampled, then the correspondence between satellite and ground scintillation estimates may be weak.

Acknowledgments. Work supported at UT Dallas by NASA grant NNX10AT029. AFRL would like to acknowledge the contribution of the U.S. Air Force Space Test Program in providing support for the C/NOFS program. Wavelet software was provided by C. Torrence and G. Compo, and is available at URL: http://atoc.colorado.edu/research/wavelets/ .

References

Basu, S., and S. Basu and B. K. Khan, Model of equatorial scintillations from in-situ measurements, *Radio Sci.*, *11* (10), 821-832, 1976.

Briggs, B. H., and I. A. Parking, On the variation of radar star and satellite scintillations with zenith angle, *J. Atmos. Terr. Phys.*, *25*, 339-365, 1963.

Farge, M., Wavelet transforms and their applications to turbulence, *Annu. Rev. Fluid Mech.*, *24*, 395-457, 1992.

Kumar, P., and E. Foufoula-Georgiou, Wavelet analysis for geophysical applications, *Reviews of Geophysics*, *35*(4), 385-412, 1997.

Lagoutte, D., and J. C. Cerisier and J. L. Plagnaud and J. P. Villain and B. Forget, High-latitude ionospheric electrostatic turbulence studied by means of the wavelet transform, *JATP*, *54*(10), 1283-1293, 1992.

Materassi,M., and C. N. Mitchell, Wavelet analysis of GPS amplitude scintillation: A case study, *42*, RS1004, doi:10.1029/2005RS003415, 2007.

Retterer, J. M., Forecasting low-latitude radio scintillation with 3-D ionospheric plume models: 2. Scintillation calculation, *J. Geo. Res.*, *115*, 03307, 2010.

Rino, C. L., A power law phase screen model for ionospheric scintillation, 1. Weak Scattering, *Radio Sci.*, *14*, 1135-1145, 1979a.

Rufenach C. L., Ionospheric scintillation by a random phase screen: Spectral approach, *Radio Sci.*, *10*,155-165, 1975.

Rufenach, C. L., Errata, *Radio Sci.*, *11*, 71, 1976.

Singh, M. and Szuszczewicz, E. P., Composite Equatorial Spread F Wave Number Spectra from Medium to Short Wavelengths, *J. Geo. Res.*, *89*, 2313–2323, 1984.

Stoneback R. A., R. A. Heelis, A. G. Burrell, W. R. Coley, B. G. Fejer, and E. Pacheco, Observations of quiet time vertical ion drift in the equatorial ionosphere during the solar minimum period of 2009, *JGR*, *116*, A12327, 2011.

Torrence, C., and G. Compo, A practical guide to wavelet analysis, *Bull. Am. Meteor. Soc.*, *79*,61-78, 1997.

A. W. Wernik, L. Alfonsi, and M. Materassi, Scintillation modeling using in situ data, *Radio Sci.*, *42* , doi:10.1029/2006RS003512, 2007.

A. W. Wernik, Wavelet transform of nonstationary ionospheric scintillation, *Acta Geo. Polonica*, *45*(3), 237-253, 1997.

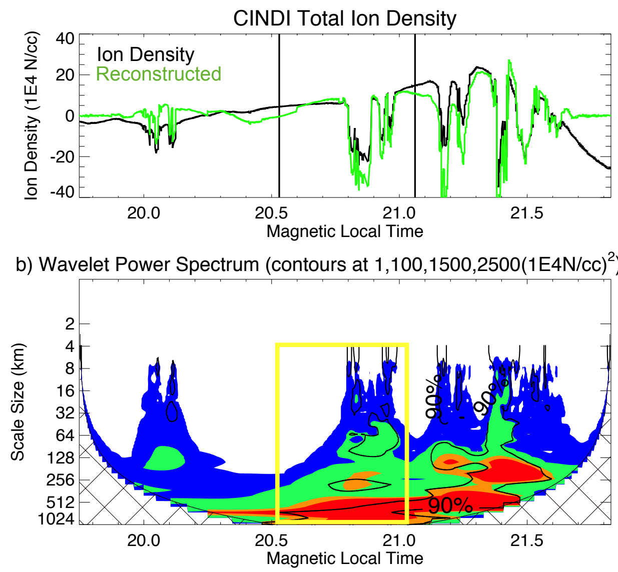

Figure 1. Example Morelet Wavelet decomposition for a portion of a satellite pass on April 19, 2009. a) The total ion density measured using CINDI is in black, the wavelet reconstruction of the perturbation in density for scale sizes above the cone of influence is in green. b) The Morlet wavelet power as a function of satellite track over a range of scale sizes is shown. The central region outlined in yellow allows investigation over a range of scale sizes free from edge effects. The perturbation waveform that corresponds to this region is denoted by the vertical lines in part a.

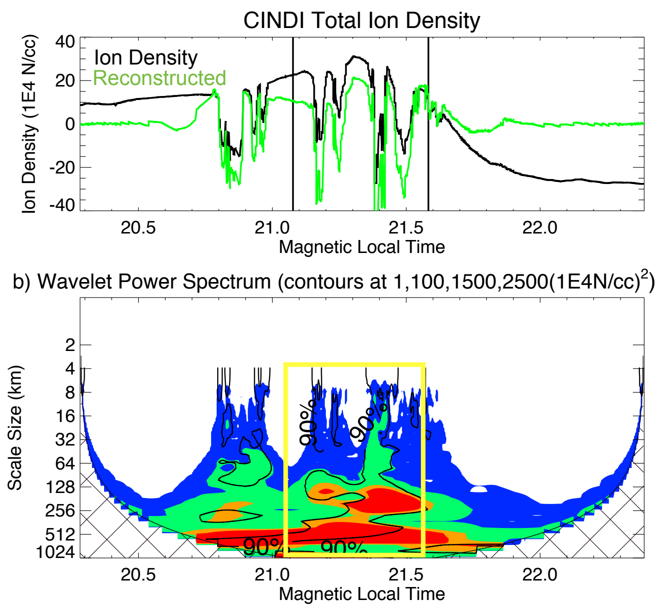

Figure 2. This figure follows the same format as figure 1, demonstrating the advancement of the finite buffer used in the wavelet decomposition by a quarter of the buffer size to extract information over a range of scale sizes free of edge effects.

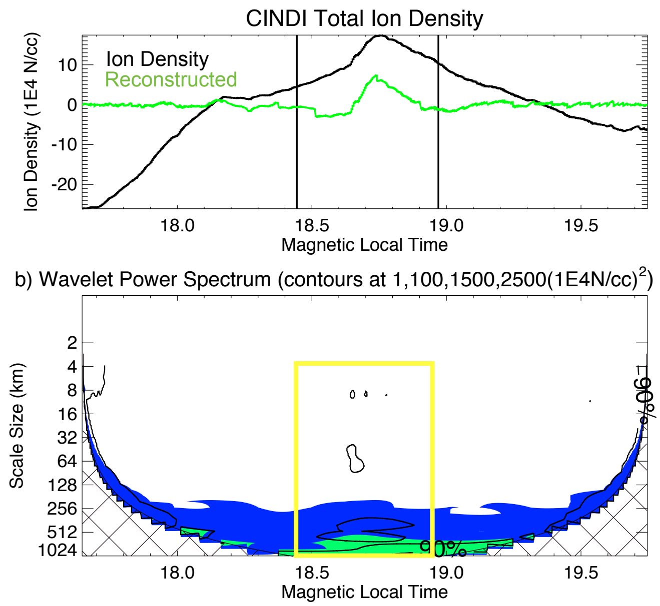

Figure 3. This figure follows the same format as figure 1. The density variation observed by CINDI on April 19, 2009 is not due to bubbles in the equatorial ionosphere. Only scale sizes less than or equal to 128 km are used in the presented scintillation estimation to limit the false prediction of scintillation for similar non-irregularity density variations.

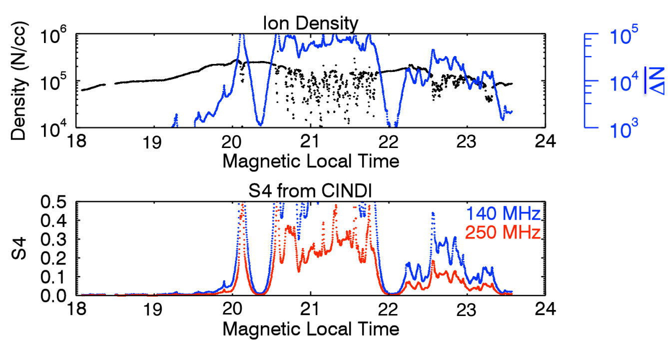

Figure 4. Top: Example C/NOFS pass on February 20, 2009. The total measured ion density is in black while the effective irregularity amplitude $\overline{\Delta N}$ is in blue and uses the right hand y-axis. Bottom: The scintillation estimation obtained using $\overline{\Delta N}$ with the method by *Basu et al.* [1976].

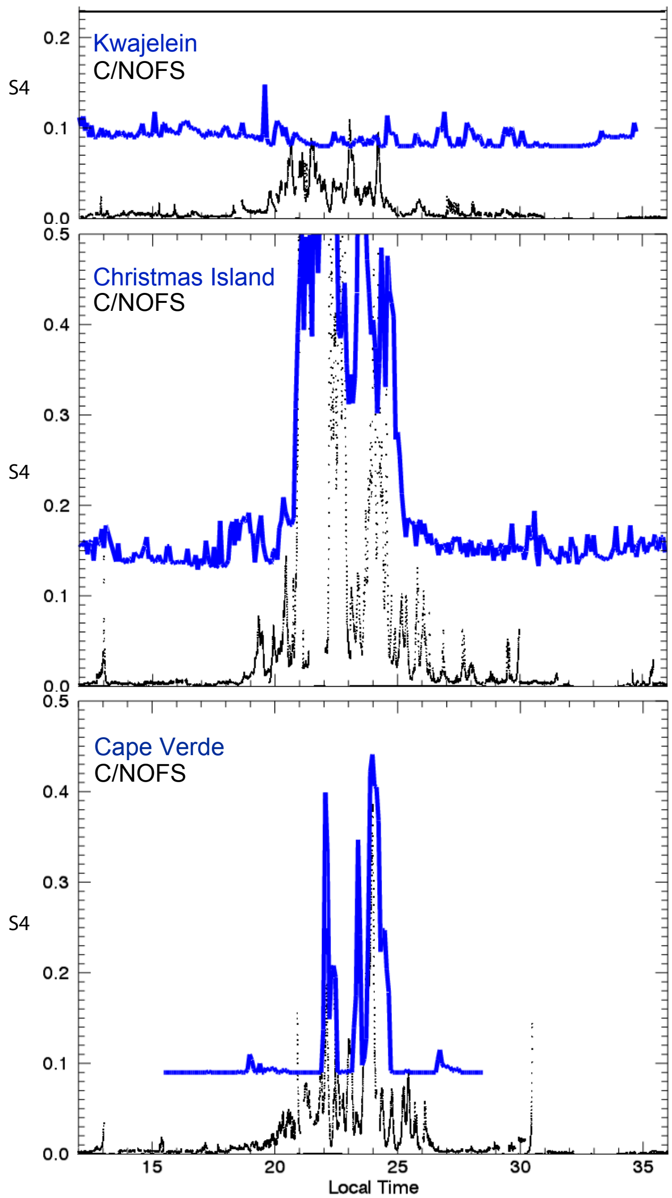

Figure 5. Top: A comparison of the S_4 index at 250 MHz at Kwajelein (top, blue) and the estimated scintillation using in-situ density measurements (black) on November 5, 2009. The C/NOFS scintillation estimation over local time is comprised of 15 passes through the Kawjelein longitude sector. Middle: Christmas Island on November 6, 2009. Lower: Cape Verde on November 6, 2009.